Future Energy
Open Access Journal
ISSN 2832-0328

February 2024| Volume 03 | Issue 01 | Pages 23-33

Journal homepage: https://fupubco.com/fuen

https://doi.org/10.55670/fpll.fuen.3.1.4

Future Publishing LLC

Review

Review of different vertical axis wind turbine modeling methods

Siavash Gitifar[1], Rahim Zahedi[2]*, Saba Ziaie[3], Amir Mohammad Mirzaei[4], Mohammad Mahdi Forootan[5]

[1]Faculty of Mechanical Engineering, Iran University of Science and Technology, Tehran, Iran
[2]Department of Renewable Energy and Environmental Engineering, University of Tehran, Tehran, Iran
[3]Department of Physics and Energy Engineering, Amirkabir University of Technology, Tehran, Iran
[4]Faculty of Materials Engineering, Tarbiat Modares University, Tehran, Iran
[5]Department of Energy Systems Engineering, Iran University of Science and Technology, Tehran, Iran

ARTICLE INFO

Article history:
Received 02 April 2023
Received in revised form
01 May 2023
Accepted 07 May 2023

Keywords:
Darrieus, Wind turbine, CFD, Modeling, Aerodynamics

*Corresponding author
Email address:
rahimzahedi@ut.ac.ir

DOI: 10.55670/fpll.fuen.3.1.4

ABSTRACT

Wind energy can be used as an inexhaustible option for human consumption. Wind turbines offer a promising solution for off-grid areas. Darrieus turbine is one of the types of turbines that can be more efficient than other types if it is used by knowing its characteristics. The complex dynamic mechanism of the flow around the machine has led to its aerodynamic optimization problems remaining complex. This article reviews the applied methods in modeling vertical axis turbines and implicitly shows the turbine operation by presenting the results of these methods. Knowing these methods is important because each has its advantages and disadvantages and should be selected depending on the purpose of the research. One of the problems with Darrieus turbines is their poor start-up, which has been little researched so far. Finally, a suitable method that can model the start-up is introduced.

1. Introduction

The focus on renewable energy sources has increased significantly in recent years due to environmental pollution, increasing energy demand, and declining fossil fuel resources. Various sources of renewable energy include biomass, solar, geothermal, hydroelectric, and wind. In the meantime, the wind has been proven to be a cheaper alternative to energy, and hence extensive research efforts have been made to improve wind power generation technology. The world has enormous potential for wind energy that can be used to generate electricity. According to research by Iran's New Energies Organization, Iran has areas with good potential for wind energy. Since wind speed is different in different parts of the country, to efficiently use wind energy, a suitable turbine must be selected with environmental conditions to have a proper economic justification [1]. Over the past 10 years, electricity generation capacity has increased from 25 GW to 200 GW [2]. The first type of man-made wind turbine is a type of drag-type vertical axis wind turbine (VAWT) used in the Sistan region [3]. Although VAWTs were the first turbines used by humans, modern-day researchers have shown no interest in them because they cannot generate electricity on a large scale. In recent decades, horizontal axis wind turbines (HAWT)s have been extensively researched, and a large part of the installed capacity of wind turbines is related to this type of turbine [4]. However, research on VAWT continued in parallel on a smaller scale. Solving the main problems related to VAWTs, such as blade lift force, blade failure due to oscillating force and oscillating wind, etc [5, 6]. are some common previous studies, but more research is needed. VAWTs are currently not economically attractive on a large scale [3]. However, VAWT is a way to generate energy in locations away from the main distribution line or where wind farms cannot be used due to environmental issues, so small-scale dispersed generation units are preferred. For this reason, mass production of VAWTs has only recently begun as a small-scale production unit [7]. Scientists have created various configurations of this type of turbine and have used different methods for their studies. In this paper, the details of these techniques and configurations are examined, along with the important findings of researchers about VAWTs, and a new method for

Nomenclature:

A	projected frontal area of turbine (m^2)	C	blade chord (N/m^2)
C_d	blade drag coefficient	C_D	turbine overall rotor drag coefficient
C_{DD}	rotor drag coefficient $F_D/\rho A V_\infty^2$	C_n	normal force coefficient
C_l	blade lift coefficient	C_p	Power factor
F_t	tangential force	F_n	normal force (in the radial direction)
F_D	turbine overall drag force	H/C	aspect ratio
F_{ta}	average tangential force	H	height of turbine
F^*	reduced frequency	P	Power (w)
V	speed (m/s)	W	Relative speed (m/s)
V_c	chordal velocity component	V_n	normal velocity component
V_{au}	induced velocity in the upstream side	V_{ad}	induced velocity in the downstream side
u	induction coefficient in the upstream	u'	induction coefficient in the downstream

Greek signs

α	AOA (rad)	ρ	density (kg/m^3)
ω	angular velocity (rad/s)	σ	solidity
$\lambda = R\omega/V_\infty$	tip speed ratio		

Subscript

a	induction	gen	generator
d	downstream condition	u	upstream condition

Abbreviations

HAWT	horizontal axis wind turbine	VAWT	vertical axis wind turbine
AOA	angle of attack	TSR	tip speed ratio
MST	multiple streamtube	DMST	double multiple streamtube
BEM	momentum models	PIV	particle image velocimetry
Kω-SST	Kω-shear stress transport	CFD	computational fluid dynamics
URANS	unsteady Reynolds-averaged Navier-stokes	LES	large eddy simulation
DES	detached eddy simulation	RFM	reference frame method
SMM	sliding Mesh Method	CFL	Courant_Friedrichs-Lewy number

investigating this type of turbine will be proposed and compared with previous samples.

2. Wind turbines configuration

Differences in the shape and efficiency of wind turbines cause differences in the appropriate conditions for their use. In this section, we will review the types of turbines and compare them.

2.1 HAWTs

A group of turbines whose axis of rotation is horizontal. Early types include German and American windmills [6]. The first wind turbine in the United States was commercially used in 1931 by Charles Brush to generate electricity [5]. But modern VAWTs (Figure 1), which are used commercially for wind farms to generate electricity, usually have three blades that provide the force needed to rotate the rotor by lift force. The blades are positioned in the wind direction by a computer-controlled motor. At the top of the tower, there is a gearbox and a generator, and the blades are connected to this part. These turbines have been a major part of the contemporary history of wind energy technology and are a common commercial type. Although the efficiency of these turbines is high, it also has disadvantages that will be mentioned in the next section [8].

2.2 Drag-type VAWTs

Sistan wind turbine, which is also the first type of wind turbine, falls into this category, but the most famous type of this category, which has a higher efficiency than other cases of drag-type, is the Savonius rotor, whose name is derived from the name of its Finnish designer. This type of turbine, which is a drag-type and vertical axis, was first tested in 1925. This rotor was very popular in the 1960s and 1970s due to its simple construction and production, high starting torque, and ability to accept wind force from all directions. However, it has some disadvantages, such as high weight, low efficiency (15-19 percent), high torque changes on the axis of rotation, and wind from low latitudes which made it out of the spotlight over time made [9, 10]. The mechanism of this type of turbine is such that the wind drag force in the concave part of the turbine is more than the convex part, and therefore it will cause the rotor to rotate [11]. After passing through the concave part, the fluid enters the other half of the rotor to apply a force against the direction of wind flow and in the direction of rotation of the rotor. Regardless of the drag force in the convex part, the turbine output capacity is calculated as Eq. 1 [5, 10, 12].

$$P = F_d u = \frac{1}{2}\rho A(v_{air} - u_{turbine})^2 C_D u_{turbine} \tag{1}$$

And maximum power factor in the blade tip speed ratio (TSR) 1/3:

$$C_P = \frac{P}{\frac{1}{2}\rho A v^3} = C_D \frac{4}{27} \tag{2}$$

By comparing the maximum output power of the drag-type turbine with the Betz limit, the inherent weakness of the efficiency of the drag-type turbines is simply revealed. Even if we use the maximum drag coefficient, which belongs to the wind-facing hemisphere ($C_D = 1.3$), the maximum output power coefficient is 0.193, which is much lower than the Betz limit. Another disadvantage of drag turbines is the efficient use of half of the space occupied by the rotor. Although wind technology began with drag-type mills, in practice, these inherent flaws have hindered the development of more advanced species [13, 14].

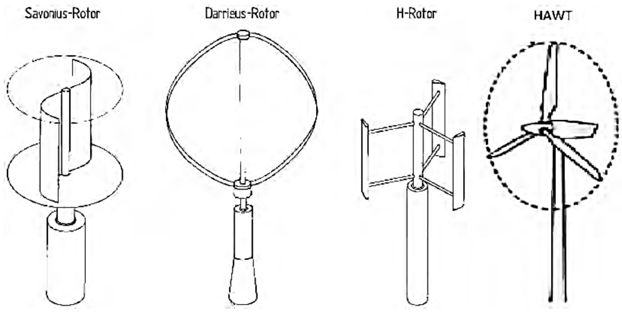

Figure 1. Different types of conventional commercial VAWTs [18]

2.3 Lift-type VAWTs

The turbine was invented in 1931 by Jean Marie Darrieus, a French engineer [6]. This turbine is of lift type, which means that, unlike the Savonius turbine, the lift force causes the turbine to rotate, and the drag force has a deterrent effect (Figure 1). The rotation speed of the Darrieus turbine is many times faster than the wind speed it blows. Therefore, the output torque of this turbine is low, and its rotation speed is high. Theoretically, this turbine has the same efficiency as the usual and commercial type of wind turbines, which in practice, considering the design limitations and resistance of the structure, it is difficult to achieve its efficiency. Using the lift force, the blade can move faster than the wind, thus producing more power [15]. The ratio of the blade tip to wind speed is a comparative indicator for wind turbines. This ratio is approximately 7 for turbine blades with maximum lift power, while 0.3 for blades with pressure drag [16, 17]. Figure 2 shows a comparison between turbine efficiencies.

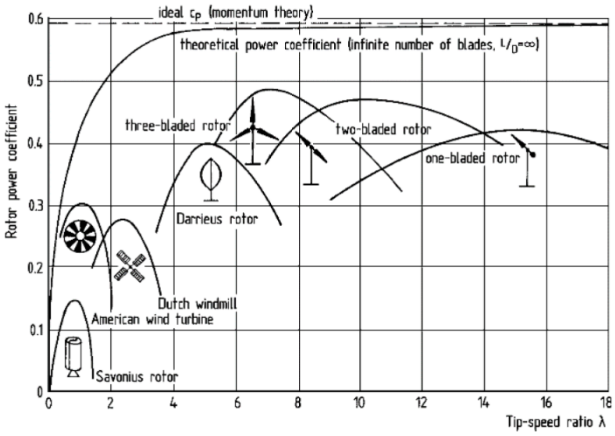

Figure 2. Comparison of the power factor of different wind turbine

When the airfoil moves in a circular path, it changes the relative speed of the wind relative to the airfoil, which ultimately produces a variable angle of attack (AOA). This wind movement on the airfoil produces lift force and, thus torque. When the airfoil rotates around the main axis and passes through the opposite point, the AOA of the airfoil becomes negative, and thus the airfoil production force continues to produce torque by the direction of rotation [19, 20]. In this rotor, the AOA with rotation is constantly changing. Therefore, in the front and back of the device, according to the wind direction, the maximum AOA and consequently, the most torque is produced. These pulsed torques make the design process complicated, and at some rotational speeds, the natural frequency of the blades equals this frequency, and this causes resonance and destruction of the device. Therefore, in design, these modes should be considered [19, 20]. Unlike HAWTs, where most of the weight of the blade structure is in the wheel bowl, in this rotor, most weight is located at the end of the arms [21]. Therefore, in this mechanism, large centrifugal forces are generated, and consequently, many stresses are applied to the structure, which adds to the complexity of the design. One of the initiatives to reduce this force is the use of rotating wings similar to the weight of an egg (also named troposkein) so that the blades themselves are attached directly to the base [22]. The rotating blades compress the column, and the column is secured from above with retaining wires. Although the Darrieus rotor is far more practical than the Savonius rotor, it still lags far behind horizontal axis turbines in terms of benefits and costs. Table 1 compares the mentioned rotors [23].

Table 1. Comparison of advantages and disadvantages of turbines

Cases	HAWT	Darrieus	Savonius
The shape of the blade	complicated	simple	simple
Rectifier mechanism	needs	needless	needless
Ability to change the angle of the blade	yes	yes	no
Large-scale construction	Yes	Yes	No
Rotor weight bearing	medium	low	high
Noise	high	low	low
Generator and gearbox location	top of the tower	ground	ground
Auto start	yes	weak	yes
Foundation	complicated	simple	simple
Ideal power factor	high	high	low
Maintenance costs	high	low	low
Research done	much	little	little
Structure set	complicated	simple	simple

3. Aerodynamic solution methods

Although the flat-blade Darrieus turbine is one of the simplest types of wind turbines, its aerodynamic study is a bit complicated. Before comparing the existing designs for aerodynamic study, the equations used in these studies are introduced. The flow velocity is not constant upstream and downstream (Figure 3). The component of cord velocity and normal velocity is obtained as follows [24, 25].

$$V_c = R\omega + V_a cos\theta \quad (3)$$

$$V_n = V_a sin\theta \quad (4)$$

In which, V_a is the axial induction velocity that passes through the rotor, ω rotor angular velocity and a is the rotor placement angle. According to Figure 3, the AOA can be calculated from the following equation [26].

$$a = \tan^{-1}\frac{V_n}{V_c} = \tan^{-1}\frac{\sin\theta}{\frac{R\omega/V_\infty}{V_a/V_\infty}+\cos\theta} \quad (5)$$

Also, the relative velocity on the blade is obtained as follows.

$$\frac{W}{V_\infty} = \frac{W}{V_a} * \frac{V_a}{V_\infty} = \frac{V_a}{V_\infty}\sqrt{\left[\left(\frac{R\omega}{V_\infty}/\frac{V_{au}}{V_\infty}\right) + \cos\theta\right]^2 + sin^2\theta} \quad (6)$$

The direction of lift and drag force, its radial and angular components, and the force coefficients in the angular and radial direction shown in Figure 3 are calculated as follows from the lift and drag coefficients obtained from the laboratory result [27].

$$C_t = C_l \sin\alpha - C_d \cos\alpha \quad (7)$$

$$F_t = \frac{1}{2} C_t \rho C H W^2 \quad (8)$$

Given that Eq. 6 is written in terms of position, then the mean angular force can be defined as follows.

$$F_{ta} = \frac{1}{2\pi}\int_0^{2\pi} F_t(\theta)\, d\theta \quad (9)$$

And the output power is obtained as follows.

$$P = F_{ta} R N \omega \quad (10)$$

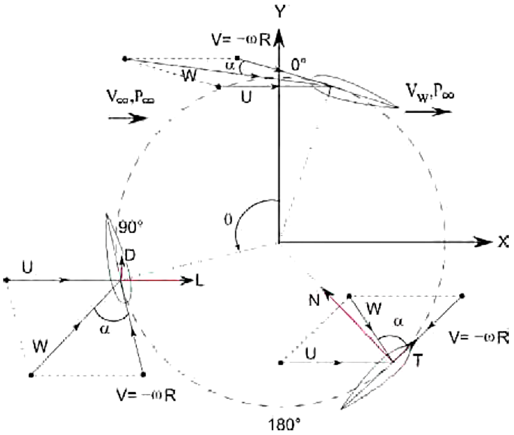

Figure 3. Velocities and forces on the Darrieus rotor [27]

In the past, several mathematical models based on several theories have been used to predict the performance and design of the Darrieus turbine in various studies. According to research conducted by Islam [28], the most and best-validated models are divided into three categories:

- Momentum models (BEM)
- Vortex model
- Cascade model

Of course, none of these three models will meet all the key performance metrics.

3.1 Momentum models (BEM)

These models have been introduced in different ways, but the basis of these models is that by placing aerodynamic forces in the direction of flow with momentum changes, the induced speed during flow will be obtained. The most important problem of these models is that they do not give a good answer for high TSR and high solidity because solving momentum equations alone is not enough [28]. In 1974, Templin [29] introduced the single streamtube (SST) model, which was the first and simplest. This model was first registered for the windmill but later expanded to the Darrieus turbine. In this theory, it is assumed that the induced velocity is constant along with the rotor and is obtained from the equality of the drag force along with the flow by a momentum change in this direction [30]. This theory pays attention to the effect of airfoil failure [31]. Thus, the effect of geometric variables such as solidity and aspect ratio as well as the effect of zero lift-drag coefficients are considered qualitative features in this theory, but the sheer effects of wind in this model are not considered [28]. According to Gluert's actuator disk theory [28], the uniform velocity passing through the rotor is equal to the average velocity upstream and downstream (Figure 4a). All these calculations are done by this model for a blade that equates the chord length of this blade to the sum of the blade lengths. The drag force in the flow direction is the result of momentum change in this direction, and by defining the rotor drag coefficient in Eq. 10, we have:

$$F_D = m(V_\infty - V_w) \quad (11)$$

$$C_{DD} = \frac{4(V_\infty - V_a)}{V_a} \quad (12)$$

$$\frac{V_a}{V_\infty} = \left(\frac{1}{1+{C_{DD}}/{4}}\right) \quad (13)$$

The total torque for the turbine will be obtained from Eq. 4-9 by placing $\frac{V_a}{V_\infty}$ in Eq. 13 during an iterative process. This model can calculate the overall efficiency for the low load mode, but according to Wilson's results, it always achieves more output power than the laboratory results because the velocity on the downstream and upstream are assumed to be the same. This difference in results increases with increasing solidity and increasing TSR [28]. In 1947 Wilson [32] introduced the multiple streamtube (MST) model. In this model, the volume swept by the turbine is divided into several streamtubes side by side. The aerodynamic dependence of the parallel streamtubes is shown in Figure 4b Previous equations are written for each streamtube. In this model, the changes in induced velocity in front of the disk are considered in both vertical and horizontal directions. Thus, this model also includes wind shear effects [28, 33]. Wilson recommended the equation for the calculation of induced velocity as Eq. 14, taking into account only the lift force.

$$\frac{V_a}{V_\infty} = 1 - \left(\frac{k}{2} * \frac{NC}{R} * \frac{R\omega}{V_\infty} * \sin\theta\right) \quad (14)$$

In 1981, Paraschivoiu [34] introduced the double-multiple streamtube (DMST) model. In this model, calculations are obtained for the two upstream and downstream sections according to Figure 4c The flow of air passing through the tube passes through two actuator disks in a row.

$$V_{au} = uV_\infty \quad (15)$$

$$V_e = (2u-1)V_\infty \quad (16)$$

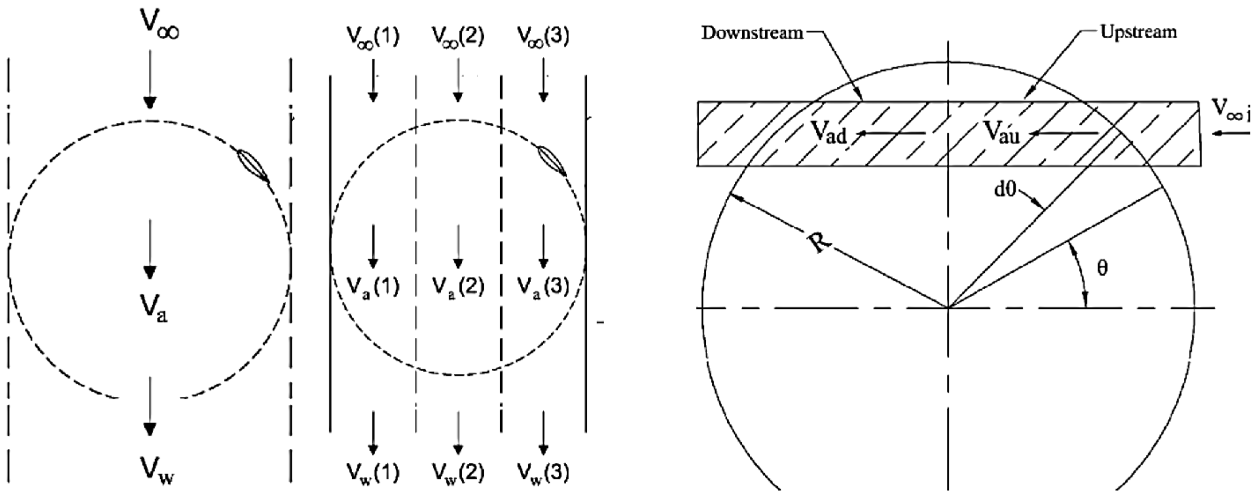

(a) (b) (c)

Figure 4. (a) SST model, (b) MST model, (c) DMST model [28]

$$V_{ad} = u'(2u-1)V_\infty \tag{17}$$

In which, V_{au} and V_{ad} are induced velocity in upstream and downstream side and, V_e in the wake velocity. Also, u is the induction coefficient in the upstream, and u' is the induction coefficient in the downstream and is always $u' < u$. The turbine's overall drag force in the direction of the stream is obtained from the following equation.

$$F_D = \frac{\sigma}{2\pi}\int_{-\frac{\pi}{2}}^{\frac{\pi}{2}} \frac{W^2}{V_\infty}\left(C_N\frac{cos\theta}{|cos\theta|} - C_T\frac{sin\theta}{|cos\theta|}\right)d\theta \tag{18}$$

This method was able to solve one of Wilson's problems, which was the equality of the induction velocities of the front and rear blades, but problems with convergence (especially downstream and high TSR) appeared [28]. The results of these methods showed (Figure 5 and Figure 6) as the TSR increases, the turbine power coefficient increases to reach an optimal TSR. After this, the power factor will decrease with increasing TSR. Paraschivoiu was also able to study the effect of solidity as shown in Figure 7. His results showed that with increasing solidity, the power coefficient in TSR reaches its optimal value.

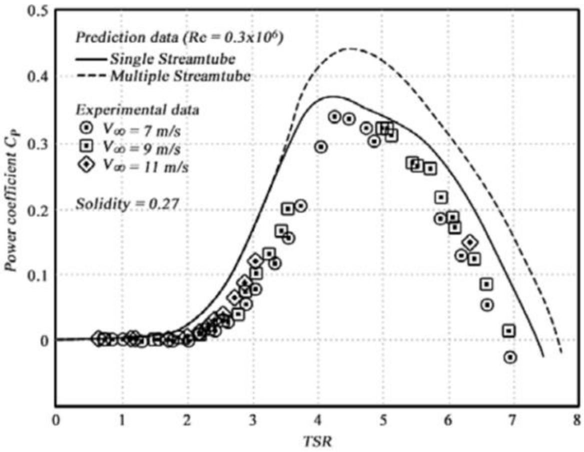

Figure 5. Comparison of SST and MST models with laboratory information [35]

In 2013, Batista et al. [35]. made a comparison between the models as shown in Figure 5 and Figure 6. His results showed that the DMST model has the closest adaptation of the three models to laboratory information but also, has the most difficult convergence conditions. All three models at higher solidity and higher TSR predict higher results from laboratory data. With the help of these methods, it was possible to obtain the main aerodynamic properties with low calculations, but these methods, which were not able to model the shape of the flow, are unable to investigate the causes of phenomena such as power factor reduction for TSR greater than 6. Another problem with these methods is the lack of proper airfoil information at attack angles above the stall state.

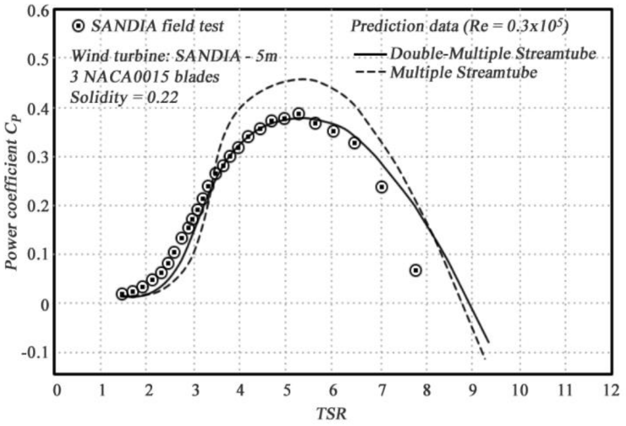

Figure 6. Comparison of multiple and DMST models with laboratory information [35]

3.2 Vortex model

The vortex model is based on potential flow. This model calculates the velocity field around the turbine through the influence of velocity in the wake of the models. Turbine blades are expressed as concentrated vortexes. The strength of these vortexes is obtained by collecting airfoil coefficient data and calculating the relative flow and AOA. In VAWTs, the blade element is replaced by a substitution vortex filament or a lift-line [28]. This method is well compatible with laboratory information and was able to solve some of the problems of the previous method. Dixon's results [37] could explain that as the blade speed increases, less energy is wasted from the wind, but after exceeding 6 times the wind speed, the blade collides with the non-renewed wind flow, which reduces the power factor (Figure 8). However, this method cannot visualize the flow well and requires a lot of calculations [28, 38].

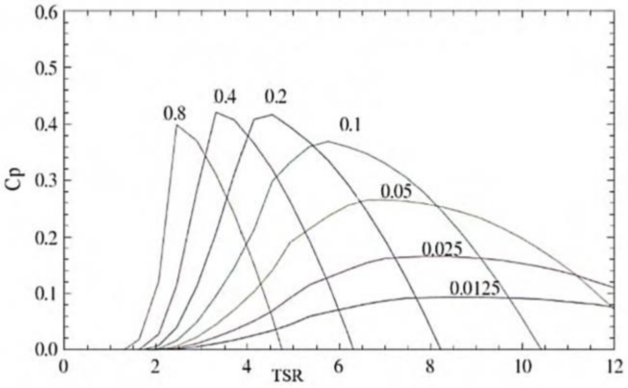

Figure 7. Turbine power coefficient curve in terms of TSR for σ=0.8 [36]

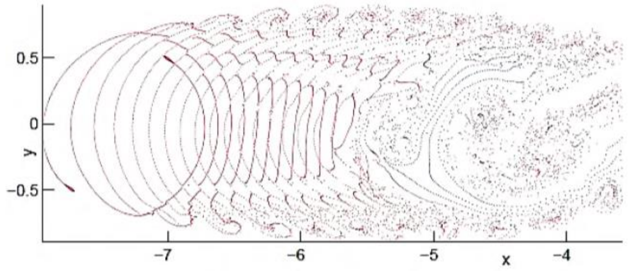

Figure 8. Displays the rise motion of the vortex method [37]

4. Flow field visualization by particle image velocimetry (PIV)

Aerodynamic models, no matter how well they predict the power and performance coefficients of the turbine, are still unable to visualize the flow field. Visualization of the flow field around the wind turbine facilitates the understanding and analysis of the aerodynamic behavior of the wind turbine, which is necessary to improve the efficiency and proper design of the device [39]. In 1999, Fujisawa et al. [40] visualized the flow field in an area of the Darrieus rotor during dynamic stalls by injecting dye. In this method, the dye was injected into the fluid stream, and the flow model was observed through the dye path. They used the PIV method and the regional imaging technique to measure the average velocity distribution around the blade. In PIV, tracer particles with a specific gravity close to the fluid flow are injected into the fluid without affecting its velocity. These particles move at the same local velocity of the fluid. Images of moving particles are taken at any given moment with the help of a digital camera, and then these images are analyzed to obtain the velocity of the fluid at that moment. They concluded that the dynamic stall phenomenon occurs due to the flow of two pairs of vortices from the blades as they rotate from the rotor. At low rotor speeds (TSR<3), the AOA is variable and dynamic stall occurs [39]. In 2014, Danao et al. [41]. compared the turbulence models Kϵ and Kω-SST with laboratory results (Figure 9). Their results showed that model Kω-SST has a greater ability to model the flow around the rotor. Model $K\epsilon$ was initially introduced for high-spin currents, but over time, corrections were made to model the flow along the wall. Therefore, as previously predicted according to their results, this model is better consistent with the laboratory results around turbomachines and because it is two equations does not increase the calculations.

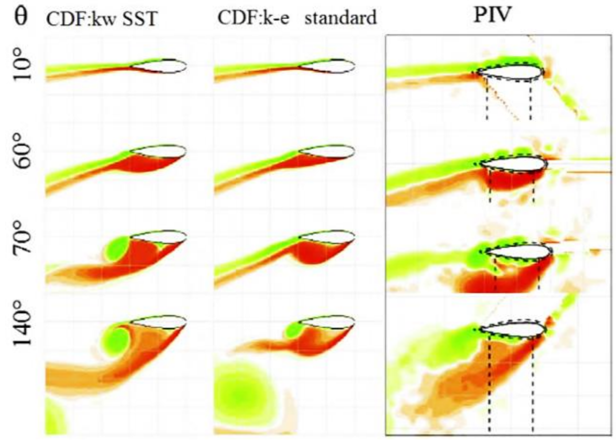

Figure 9. Flow visualization using Kϵ, Kω-SST and PIV [41]

In addition, they examined the effect of wind blowing on an unsteady basis. Their results showed that if the wind enters the turbine in an oscillating manner, the optimal of the blades differs and occurs in less than the steady-state (Figure10).

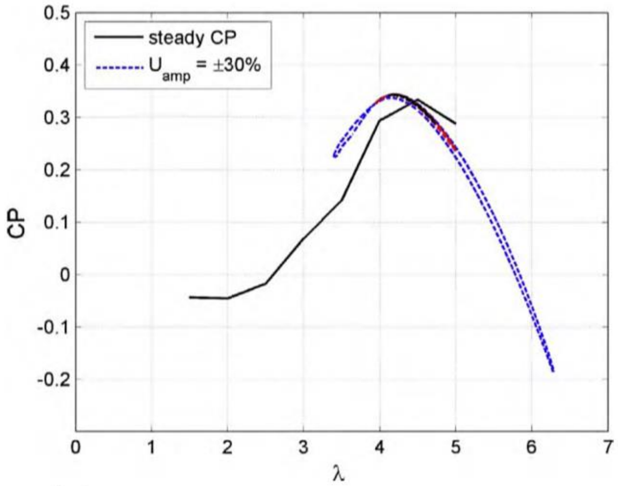

Figure 10. Power factor curve for both steady and oscillating wind modes [41]

5. Computational fluid dynamics (CFD) methods

CFD is now becoming a powerful tool in fluid mechanics that analyzes and solves fluid flow problems using numerical methods and algorithms with the help of electronic computers [42]. Using CFDs can save time and costly testing and can also be used to improve VAWT analysis. A well-tuned CFD model can simulate actual flow conditions that can produce results consistent with laboratory outputs.

Therefore, design optimization can be done before entering the construction stage [43]. CFD analysis has been widely used to determine power factor in different types of wind turbine configurations. The CFD technique for visualizing the flow field of a VAWT can be seen in Allet's early work [44]. Debnath et al. [45] used the CFD to test the Savonius-Darrieus rotor, which is more capable of starting than the Darrieus rotor. In 2010, Wang et al. [46] used two unsteady Reynolds-averaged Navier-stokes (URANS) models with standard Kω and Kω-SST to simulate the phenomenon of the dynamic stall at low Reynolds (Re≈105). After comparing the results of this model with the experimental model, they found that model Kω-SST is better than standard Kω. Model Kω-SST shows the main features of the dynamic stall phenomenon, such as the aerodynamic residual load and the flow structure of the vortexes of the front of the airfoil. Large eddy simulation (LES) models are more advanced and more powerful than URANS models. They require more computation time but their results are more accurate. Among the two models, detached eddy simulation (DES) and LES, the DES model is a better model due to the greater agreement of the results with the experimental results. The DES model is a combination of the LES model and the URANS model. This model not only has a lower computational cost than the LES model but also models the wall area more accurately [47-49]. To test turbines by the CFD method, in addition to the equations governing the fluid flow field, the movement of the turbine blades must also be considered. In general, turbine motion is modeled in three ways: stationary rotor, constant speed rotor, and accelerated rotor [50].

5.1 Stationary rotor

In this method, it is assumed that the rotor is fixed and the resulting current and torque are obtained for several angles of the fluid field. Menet et al. [51] compared the flow field for several different angles of the two Savonius turbines but did not obtain good values for the power factor compared to the laboratory data. Of course, this method is not very useful for lift-type turbines such as Darrieus due to the high importance of the relative speed on the rotor. In 1999, Allet et al. [44] investigated the behavior of an airfoil at higher angles of the stall for which it did not have adequate laboratory information at rest and combined aerodynamic methods to obtain the power factor for Darrieus turbines. Of course, their data always showed a lower power factor than laboratory data, due to the inability of this method to consider dynamic stall resulting from its static study [50].

5.2 Constant speed rotor

In general, three methods of reference frame method (RFM) and sliding mesh method (SMM), and dynamic mesh are often used to study turbomachines that have moving parts [52]. In the RFM method, which is also the simplest method, the relative coordinate system is adapted to the rotor, and instead of the mesh deformation, it is assumed that the boundary conditions are rotating around the axis and the momentum equations for the rotating device are correct. Of course, this method is not very useful for analyzing turbomachines because it solves the problem steadily and does not give a good analysis of the problem, which is generally transient [8, 53, 54]. Korobenko et al. [55] used a complete method known as SMM. In this method, unlike RFM, the mesh shape will change. Amet et al. Divided the solution area into a fixed part and a rotating part in which the rotor was located. For each subdomain, the governing equations are solved and related by Eq. 19 and 20 through our boundary which is known as the interface boundary.

$$U_M - U_S = 0 \tag{19}$$

$$(2\mu\varepsilon U_S - P_S I)n_S + (2\mu\varepsilon U_M - P_M I)n_M = 0 \tag{20}$$

In which, I is the unit tensor, S and M are the fixed amplitude and the moving amplitude, respectively, and n are the unit vectors perpendicular to the outside. In this solution, the rotational amplitude equations are given a stationary angular velocity and the forces and torque on the turbine are calculated at each time step. In 2009, Amet et al. [56] used the same method to investigate the effect of a vortex on the operation of a Darrieus turbine. By defining the reduced frequency as Eq. 21, they introduced the ratio of the time of fluid movement on the blade to the time scale of the intensity of changes in the AOA.

$$F^* = \frac{C}{R} * \frac{1}{\lambda - 1} * \frac{1}{2\alpha_{max}} \tag{21}$$

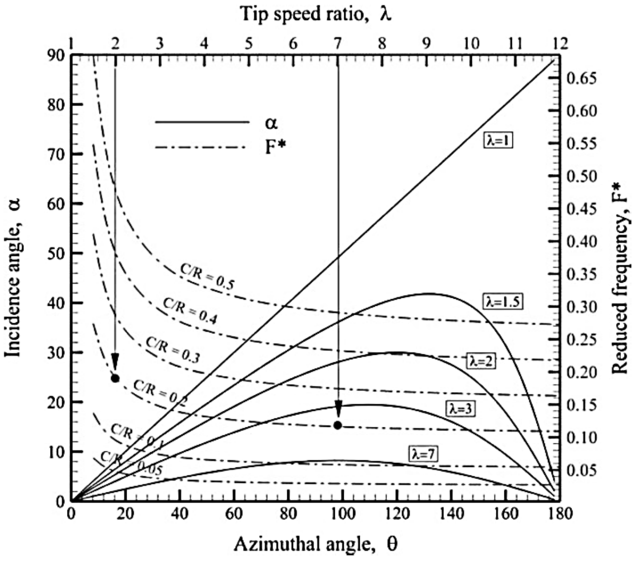

Figure 11. α curve in terms of θ for different λ and F* in terms of λ for different solidities [56]

For high F* (greater than 0.05), if the AOA is greater than the static state, the device is prone to strong dynamic failure with vortex separation. Figure 11 shows two curves, first α in θ for different λ and the other F* in λ for different solidities. The first curve shows that 2<λ<6, results in the 9.5<AOA<30 degrees. These angles are higher than the 12 for the static stall. For λ>5, the AOA does not exceed 12 in the whole half. The second curve shows that if the two conditions λ>5 and C/R>0.1 are met, a strong dynamic failure is expected. Amet compared the separated vortexes for the two AOA 2 and 7. Figure 12 shows that the pair of vortexes that are clockwise and counter-clockwise detached from the blade when it is upstream, and in the downstream part of the rotor may collide with the blade, causing a drop in the blade lift coefficient. Of course, whether this reduction in lift factor reduces the rotor power depends on whether the torque in that area is positive or negative. Figure 13 shown for λ=2, shows an oscillation drop-in area 8 due to the movement of a vortex along the stream, which continues in area 15. Figure 14 shows that if the TSR increases, fewer vortexes are formed with lower power and have little effect on the lower blade.

Figure 15 shows the lift factor in a complete rotor rotation in λ=2. According to this diagram, with the increase of α, the oscillation caused by the collision of vortexes with the blade is no longer observed. Amet also showed that by increasing the TSR, the flow is not able to repress the pressure, and the turbine efficiency decreases [56].

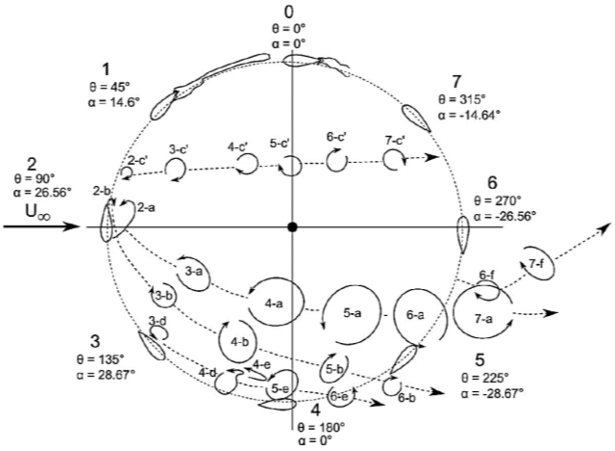

Figure 12. The path of separated vortexes in λ=2 [56]

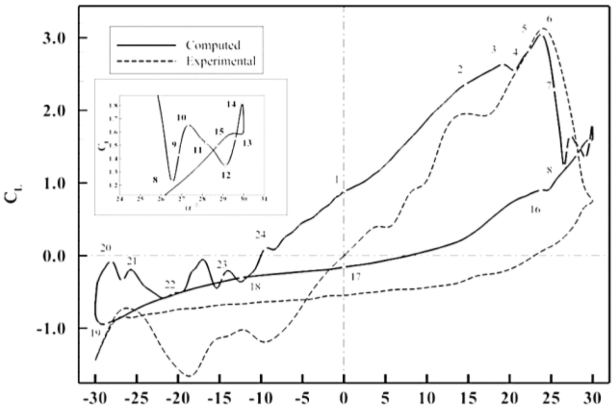

Figure 13. Lift coefficient in a complete revolution, in λ=2 [56]

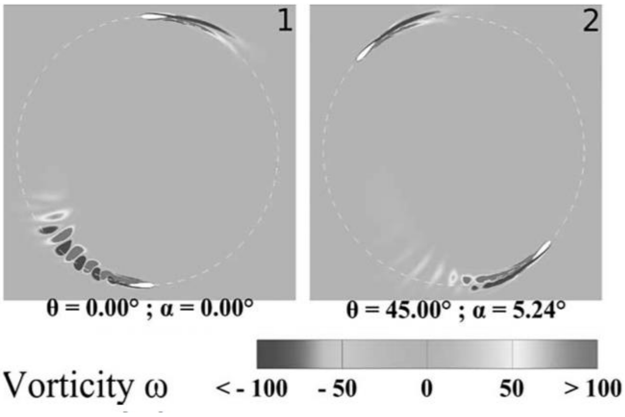

Figure 14. The path of separated vortexes in λ=7 [56]

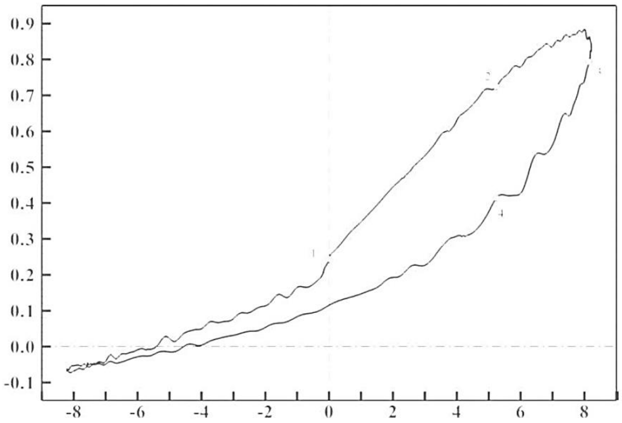

Figure 15. Lift coefficient in a complete revolution, in λ=7 [56]

6. One degree of freedom rotor

According to studies, all the research that has been done so far has been done with the constant rotation speed method, and only Alessandro in 2010 [57] and Jaohindy in 2013 [58] used the accelerated rotation speed for the Darrieus rotor. In this method, the torque applied to the turbine causes proportional acceleration and motion in the turbine, which means that the rotor motion will be obtained by coupling the Lagrangian equations of CFD and the Euler equations of the rigid body. Figure 16 shows the dynamic solution flowchart, which consists of three main processes; Solve fluid flow, rotor processing, and mesh deformation processing. In other words, according to this method, the motion of a solid body is coupled by solving the flow field. According to the flowchart, the initial angular velocity is first considered zero. Then the equations governing the fluid field are solved, and the forces acting on the rotor are calculated. In the next step, the angular acceleration will be calculated by the code written according to Eq. 22.

$$J_{oz}\ddot{\theta} + M_{oz} \tag{22}$$

$$M_{oz} = M_p + M_\tau + M_f \tag{23}$$

$$M_f = \sum_{K=0}^{H} a_k w^k + M_{gen} \tag{24}$$

In which, J_{oz} is the moment of inertia of the rotor around the z-axis, M_p is the torque due to pressure, M_τ is the torque due to viscous forces and, M_f is the torque generated by the generator load, which also includes mechanical friction. It should be noted that M_τ and M_p are obtained by calculations from the fluid flow field calculated in the previous step, and M_p is obtained by Eq. 24, whose coefficients are taken into account by the laboratory information. Using the acceleration obtained in this step, the new location of the rotor is determined in the next time step. In the next step, the appropriate mesh is deformed with the new location of the rotor by the SMM method [58]. Since the time step is a function of the Courant_Friedrichs-Lewy number (CFL) number and the rotation speed of the rotor, it is recommended to change the time step according to the rotor for the appropriate computational volume. Fluent software can calculate the time step in each time step by writing code [53, 59, 60].

As mentioned, the main weakness of the Darrieus rotor is its initial start. DeCost et al. [61] by examining the start of the Darrieus rotor by the PID method found that the drag forces had a greater effect on the start of the rotor than the lift force, which may even rotate in the opposite direction, but after increasing speed and the effects of lift force, the rotor accelerates in the right direction to reach its working speed. Flow field studies can be useful to obtain optimal starting conditions. Conventional methods that keep the rotor speed constant can certainly not work for this mode, and there is a need for a method that can study the rotor speed based on actual conditions. In addition to the starting period of the turbine in the rotor operating mode, the speed is not constant even during one rotation. Based on the results of Jaohindy et al. [58] it can be said that after passing the starting period during a rotation, due to the change in torque at different angles, different accelerations are obtained from Eq. 22, and as a result, we have different angular velocities during a rotation. According to Eq. 6, angular velocity strongly affects the relative velocity and lift force, which results in torque with an oscillating amplitude greater than the real state because the rotor speed is obtained from the flow conditions.

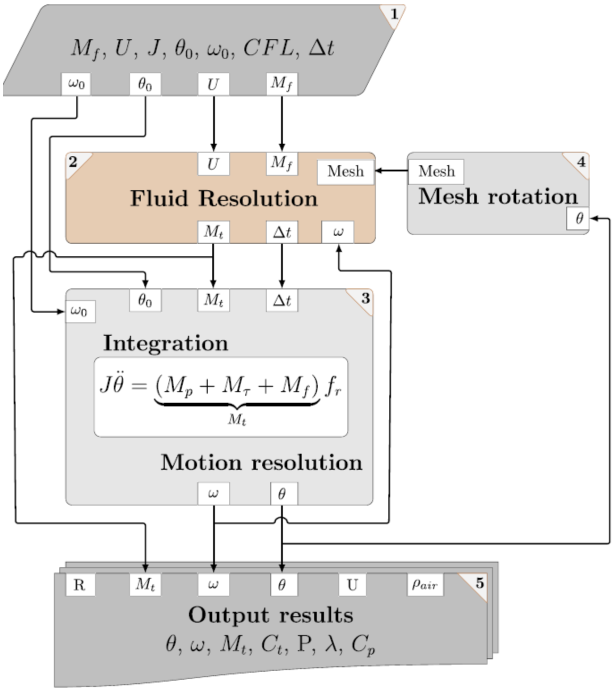

Figure 16. The flowchart is proposed for the dynamic solution method [58]

7. Conclusion

In this article, wind turbines were first compared. Darrieus turbine, along with many advantages, has a problem of starting and efficiency less than HAWTs, which can be widely used if these problems are solved. The various methods used to evaluate the aerodynamic characteristics of VAWTs were reviewed. Meanwhile, momentum models are cheap but inaccurate and are considered suitable for iterative optimization algorithms. The Vertex model has acceptable accuracy but has a high computational cost, which has prevented the use of these models. Of course, with the advances made, these models also have some ability to imagine the flow. Many CFD studies have been performed on Darrieus turbines that have been able to visualize the flow field well to understand the aerodynamic phenomena around these turbines. Understanding the flow is necessary to optimize the turbine, but most researches have assumed that the rotor speed is constant. In general rotor researches, this simplification does not cause a significant error, but these models are incapable if special conditions such as the start time of the rotor should be examined. Finally, it is suggested that according to an iterative algorithm, the rotor velocity be obtained as the actual torque reaction.

Ethical issue

The authors are aware of and comply with best practices in publication ethics, specifically concerning authorship (avoidance of guest authorship), dual submission, manipulation of figures, competing interests, and compliance with policies on research ethics. The authors adhere to publication requirements that the submitted work is original and has not been published elsewhere in any language.

Data availability statement

Datasets analyzed during the current study are available and can be given following a reasonable request from the corresponding author.

Conflict of interest

The authors declare no potential conflict of interest.

References

[1] Pishgar-Komleh, S., A. Keyhani, and P. Sefeedpari, Wind speed and power density analysis based on Weibull and Rayleigh distributions (a case study: Firouzkooh county of Iran). Renewable and sustainable energy reviews, 2015. 42: p. 313-322.

[2] Moosavian, S.F., R. Zahedi, and A. Hajinezhad, Economic, Environmental and Social Impact of Carbon Tax for Iran: A Computable General Equilibrium Analysis. Energy Science & Engineering, 2021.

[3] Alom, N. and U.K. Saha, Evolution and progress in the development of savonius wind turbine rotor blade profiles and shapes. Journal of Solar Energy Engineering, 2019. 141(3): p. 030801.

[4] Bhutta, M.M.A., et al., Vertical axis wind turbine–A review of various configurations and design techniques. Renewable and Sustainable Energy Reviews, 2012. 16(4): p. 1926-1939.

[5] F. Estelaji, A. A. Aghajari, and R. Zahedi, "Flood zoning and developing strategies to increase resilience against floods with a crisis management approach," Asian Review of Environmental and Earth Sciences, vol. 10, no. 1, pp. 14-27, 2023.

[6] H. Pourrahmani, R. Zahedi, S. Daneshgar, and J. Van herle, "Lab-Scale Investigation of the Integrated Backup/Storage System for Wind Turbines Using Alkaline Electrolyzer," Energies, vol. 16, no. 9, p. 3761, 2023.

[7] Howell, R., et al., Wind tunnel and numerical study of a small vertical axis wind turbine. Renewable energy, 2010. 35(2): p. 412-422.

[8] Manatbayev, R., et al., Numerical simulations on static Vertical Axis Wind Turbine blade icing. Renewable Energy, 2021. 170: p. 997-1007.

[9] Hand, B. and A. Cashman, A review on the historical development of the lift-type vertical axis wind turbine: From onshore to offshore floating application. Sustainable Energy Technologies and Assessments, 2020. 38: p. 100646.

[10] Kim, S. and C. Cheong, Development of low-noise drag-type vertical wind turbines. Renewable energy, 2015. 79: p. 199-208.

[11] Zahedi, R. and A.B. Rad, Numerical and experimental simulation of gas-liquid two-phase flow in 90-degree elbow. Alexandria Engineering Journal, 2021.

[12] Zheng, M., et al., Effect of blade number on performance of drag type vertical axis wind turbine. Applied solar energy, 2016. 52(4): p. 315-320.

[13] Barnes, A., D. Marshall-Cross, and B.R. Hughes, Towards a standard approach for future Vertical Axis Wind Turbine aerodynamics research and development. Renewable and Sustainable Energy Reviews, 2021. 148: p. 111221.

[14] El-Baz, A., K. Youssef, and M. Mohamed, Innovative improvement of a drag wind turbine performance. Renewable Energy, 2016. 86: p. 89-98.

[15] Saat, A.F. and N. Rosly, Aerodynamic analysis of vertical axis wind turbine. Journal of Aviation and Aerospace Technology, 2019. 1(1).

[16] Wong, K.H., et al., Performance enhancements on vertical axis wind turbines using flow augmentation systems: A review. Renewable and sustainable Energy reviews, 2017. 73: p. 904-921.

[17] Li, J., et al., Aerodynamic stability of airfoils in lift-type vertical axis wind turbine in steady solver. Renewable Energy, 2017. 111: p. 676-687.

[18] Saleh, A. and B.F. Feeny, Modal analysis of a vertical-axis darrieus wind turbine blade with a troposkein shape, in Topics in Modal Analysis & Testing, Volume 9. 2019, Springer. p. 325-327.

[19] Hand, B., G. Kelly, and A. Cashman, Aerodynamic design and performance parameters of a lift-type vertical axis wind turbine: A comprehensive review. Renewable and Sustainable Energy Reviews, 2021. 139: p. 110699.

[20] Zhao, Z., et al., A review: Approaches for aerodynamic performance improvement of lift-type vertical axis wind turbine. Sustainable Energy Technologies and Assessments, 2022. 49: p. 101789.

[21] Daneshgar, S. and R. Zahedi, Optimization of power and heat dual generation cycle of gas microturbines through economic, exergy and environmental analysis by bee algorithm. Energy Reports, 2022. 8: p. 1388-1396.

[22] Roy, L., et al., Double-Multiple Streamtube Analysis of a Flexible Vertical Axis Wind Turbine. Fluids, 2021. 6(3): p. 118.

[23] Chen, J., et al., A comprehensive review of the theoretical approaches for the airfoil design of lift-type vertical axis wind turbine. Renewable and Sustainable Energy Reviews, 2015. 51: p. 1709-1720.

[24] Loth, J., Aerodynamic tower shake force analysis for VAWT. 1985. https://doi.org/10.1115/1.3267652

[25] Moghimi, M. and H. Motawej, Developed DMST model for performance analysis and parametric evaluation of Gorlov vertical axis wind turbines. Sustainable Energy Technologies and Assessments, 2020. 37: p. 100616.

[26] Wang, Z., Y. Wang, and M. Zhuang, Improvement of the aerodynamic performance of vertical axis wind turbines with leading-edge serrations and helical blades using CFD and Taguchi method. Energy conversion and management, 2018. 177: p. 107-121.

[27] Homicz, G.F., VAWT stochastic loads produced by atmospheric turbulence. 1989. https://doi.org/10.1115/1.3268335

[28] Islam, M., D.S.-K. Ting, and A. Fartaj, Aerodynamic models for Darrieus-type straight-bladed vertical axis wind turbines. Renewable and sustainable energy reviews, 2008. 12(4): p. 1087-1109.

[29] Templin, R., Aerodynamic performance theory for the NRC vertical-axis wind turbine. 1974, National Aeronautical Establishment, Ottawa, Ontario (Canada).

[30] M. V. Khah et al., "Optimal sizing of residential photovoltaic and battery system connected to the power grid based on the cost of energy and peak load," Heliyon, 2023. https://doi.org/10.1016/j.heliyon.2023.e14414

[31] Daneshgar, S. and R. Zahedi, Investigating the hydropower plants production and profitability using system dynamics approach. Journal of Energy Storage, 2022. 46: p. 103919.

[32] M. Keshavarzzadeh et al., "Estimation of NOx pollutants in a spark engine fueled by mixed methane and hydrogen using neural networks and genetic algorithm," Heliyon, 2023. https://doi.org/10.1016/j.heliyon.2023.e15304

[33] Saber, E., R. Afify, and H. Elgamal, Performance of SB-VAWT using a modified double multiple streamtube model. Alexandria engineering journal, 2018. 57(4): p. 3099-3110.

[34] Paraschivoiu, I., Double-multiple streamtube model for Darrieus in turbines. NASA. Lewis Research Center Wind Turbine Dyn., 1981.

[35] Batista, N.C., et al. Darrieus wind turbine performance prediction: Computational modeling. in Doctoral Conference on Computing, Electrical and Industrial Systems. 2013. Springer.

[36] Mandal, A., Aerodynamics and design analysis of vertical axis darrieus wind turbines. 1986, Vrije Universiteit Brussel, Belgium.

[37] Dixon, K., et al. A 3D unsteady panel method for vertical axis wind turbines. in The proceedings of the European Wind Energy Conference & Exhibition EWEC Brussels, 1-10. 2008. European Wind Energy Association EWEA.

[38] Dyachuk, E. and A. Goude, Numerical validation of a vortex model against experimentaldata on a straight-bladed vertical axis wind turbine. Energies, 2015. 8(10): p. 11800-11820.

[39] Rolin, V.F. and F. Porté-Agel, Experimental investigation of vertical-axis wind-turbine wakes in

boundary layer flow. Renewable energy, 2018. 118: p. 1-13.
[40] Fujisawa, N. and M. Takeuchi, Flow visualization and PIV measurement of flow field around a Darrieus rotor in dynamic stall. Journal of Visualization, 1999. 1(4): p. 379-386.
[41] Danao, L.A., et al., A numerical investigation into the influence of unsteady wind on the performance and aerodynamics of a vertical axis wind turbine. Applied Energy, 2014. 116: p. 111-124.
[42] Zahedi, R. and S. Daneshgar, Exergy analysis and optimization of Rankine power and ejector refrigeration combined cycle. Energy, 2022. 240: p. 122819.
[43] Chowdhury, A.M., H. Akimoto, and Y. Hara, Comparative CFD analysis of Vertical Axis Wind Turbine in upright and tilted configuration. Renewable Energy, 2016. 85: p. 327-337.
[44] M. V. Khah, R. Zahedi, M. S. Mousavi, and A. Ahmadi, "Forecasting renewable energy utilization by Iran's water and wastewater industries," Utilities Policy, vol. 82, p. 101546, 2023.
[45] Debnath, B.K., A. Biswas, and R. Gupta, Computational fluid dynamics analysis of a combined three-bucket Savonius and three-bladed Darrieus rotor at various overlap conditions. Journal of Renewable and Sustainable energy, 2009. 1(3): p. 033110.
[46] Wang, S., et al., Numerical investigations on dynamic stall of low Reynolds number flow around oscillating airfoils. Computers & fluids, 2010. 39(9): p. 1529-1541.
[47] Simão Ferreira, C., et al., Visualization by PIV of dynamic stall on a vertical axis wind turbine. Experiments in fluids, 2009. 46(1): p. 97-108.
[48] Lei, H., et al., Three-dimensional Improved Delayed Detached Eddy Simulation of a two-bladed vertical axis wind turbine. Energy conversion and management, 2017. 133: p. 235-248.
[49] Shamsoddin, S. and F. Porté-Agel, A large-eddy simulation study of vertical axis wind turbine wakes in the atmospheric boundary layer. Energies, 2016. 9(5): p. 366.
[50] Battisti, L., et al., Experimental benchmark data for H-shaped and troposkien VAWT architectures. Renewable energy, 2018. 125: p. 425-444.
[51] J.-L. Menet and N. Bourabaa, "Increase in the Savonius rotors efficiency via a parametric investigation," in European Wind Energy conference & exhibition, 2004: London, UK, pp. 22-25.
[52] Zahedi, R., et al., Potential measurement of Iran's western regional wind energy using GIS. Journal of Cleaner Production, 2022. 330: p. 129883.
[53] Parakkal, J.U., et al., Numerical analysis of VAWT wind turbines: Joukowski vs classical NACA rotor's blades. Energy Procedia, 2019. 158: p. 1194-1201.
[54] Naccache, G. and M. Paraschivoiu, Parametric study of the dual vertical axis wind turbine using CFD. Journal of Wind Engineering and Industrial Aerodynamics, 2018. 172: p. 244-255.
[55] Korobenko, A., et al., Aerodynamic simulation of vertical-axis wind turbines. Journal of Applied Mechanics, 2014. 81(2).
[56] Amet, E., et al., 2D numerical simulations of blade-vortex interaction in a darrieus turbine. Journal of fluids engineering, 2009. 131(11).
[57] D'Alessandro, V., et al., Unsteady Aerodynamics of a Savonius wind rotor: a new computational approach for the simulation of energy performance. Energy, 2010. 35(8): p. 3349-3363.
[58] Jaohindy, P., et al., Numerical investigation of airflow through a Savonius rotor. Wind Energy, 2014. 17(6): p. 853-868.
[59] Fluent, A., Ansys Fluent 12.0 Theory Guide. ANSYS Inc., Canonsburg, PA, 2009.
[60] Rezaeiha, A., I. Kalkman, and B. Blocken, CFD simulation of a vertical axis wind turbine operating at a moderate tip speed ratio: Guidelines for minimum domain size and azimuthal increment. Renewable energy, 2017. 107: p. 373-385.
[61] Decoste, J., et al., Self-starting Darrieus wind turbine. Design Project Mech, 2004. 4020.